Materials and Design 139 (2018) 89–95

Contents lists available at ScienceDirect

Materials and Design

journal homepage: www.elsevier.com/locate/matdes

# A highly-aligned lamellar structure of ice-templated $LiFePO_4$ cathode for enhanced rate capability

Wook Ki Jung [a], Changyeon Baek [a], Joo-Hyung Kim [a], San Moon [b], Dong Seok Kim [c], Young Hwa Jung [d], Do Kyung Kim [a,*]

[a] Department of Materials Science and Engineering, Korea Advanced Institute of Science and Technology (KAIST), 291 Daehak-ro, Yuseong-gu, Daejeon 34141, Republic of Korea
[b] Samsung Advanced Institute of Technology (SAIT), Suwon, Republic of Korea
[c] Nuclear Fuel Safety Research Division, Korea Atomic Energy Research Institute, 111, Daedeok-daero, Yuseong-gu, Daejeon, Republic of Korea
[d] Pohang Accelerator Laboratory (PAL), Pohang, Gyeongbuk 37673, Republic of Korea

## HIGHLIGHTS

- We introduce ice-templating method to fabricate lamellar structured $LiFePO_4$ cathode.
- Lamellar structures offer larger areas for ionic conductivity and a short mean free path of electrons.
- A highly-aligned lamellar structure showed superior rate performance during the discharge.
- The lamellar structure addresses aforementioned issues and potentially applicable to the porous electrode design.

## GRAPHICAL ABSTRACT

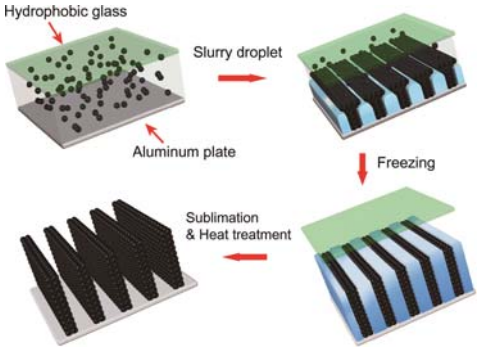


## ARTICLE INFO

*Article history:*
Received 25 July 2017
Received in revised form 1 November 2017
Accepted 2 November 2017
Available online xxxx

*Keywords:*
Ice-templating
$LiFePO_4$
Lithium-ion batteries
Highly-aligned porous cathode

## ABSTRACT

Ice-templating has been widely investigated in various energy-related fields owing to the simple and inexpensive process of this method which results highly-ordered lamellar structures. Lamellar structures offer larger active areas for ionic conductivity and a short mean free path of electrons. Here, an ice-templated $LiFePO_4$ cathode was introduced to achieve higher rate capability with a minimized carbon source. The fabricated highly-aligned porous structure demonstrates superior rate performance during the discharge process compared to electrodes which use conventional slurry casting. This enhanced performance is mainly attributed to the aligned porous structure, which facilitates the rapid transfer of electrons from the bulk to a current collector and also provides a good distribution of contact sites with Li ions in the electrolytes.



## 1. Introduction

The demand for efficient energy storage systems has led the development of advanced batteries with higher energy density levels. Li-ion batteries, as one of the most common energy storage devices, have been extensively studied as part of the effort to explore novel materials for cathodes and anodes to realize enhanced operating voltages, capacities, power, and rate capabilities, and even acceptable safety levels [1–4]. Among the parameters which determine the performance of a battery system, the rate capability is considered as most crucial, especially when devices require high-speed charge performance, such as smart mobile devices and electric vehicles [5–12]. For enhanced rate capability, the design of the electrode is crucial, as it must offer a

* Corresponding author.
*E-mail address:* dkkim@kaist.ac.kr (D.K. Kim).

https://doi.org/10.1016/j.matdes.2017.11.003
0264-1275/

**Table 1**
Carbon content of $LiFePO_4$ raw powder and carbonized LFP/PAA composite.

| Sample | Carbon content [wt%] |
|---|---|
| Raw powder (LFP-400) | 2.1 |
| After carbonization (LFP-400/carbon) | 4.4 |

**Table 2**
Specifications of the fabricated $LiFePO_4$ cathodes.

| Sample name | Preparation method | $LiFePO_4$ [wt%] | Carbon [wt%] | PVDF [wt%] | Loading [mg $cm^{-2}$] |
|---|---|---|---|---|---|
| CS_3 | Conventional slurry-cast cathode | 86.4 | 8.6 | 5.0 | 3 |
| CS_5 | | 86.4 | 8.6 | 5.0 | 5 |
| FC_3 | Ice-templated cathode | 96 | 4.0 | – | 3 |
| FC_5 | | 96 | 4.0 | – | 5 |

short mean free path of electrons and a large contact area between the active materials and the electrolytes.

The active materials used in these systems are usually coated onto a metal foil (a typical current collector) in the form of a slurry which contains conducting agents and binders along with the active materials and volatile solvents via a conventional slurry casting method [13–15]. In terms of rate performance capabilities, this conventional preparation method of electrodes using a slurry is associated with several problems, including the agglomeration and separation of the active materials during the mixing process and increased electrical resistivity mainly induced by the insulating binders used. In order to address these issues, various designs for binder-free and porous electrodes have been widely investigated to obtain high rate performance and stable cycleability [16,17].

One promising approach is to prepare highly-aligned porous structures without the use of a binder. Such an aligned structure can expand the active reaction sites to facilitate the efficient transfer of electrons through every nanostructure in the array. The void volume between the neighboring materials can also allow for easy penetration of the electrolyte, resulting in high Li-ion flux. Several studies have concentrated on developing fabrication methods for these aligned porous nanostructures [18–20]. Ice-templating, known to be an environmentally friendly and cost-effective method, is advantageous for producing aligned porous structures with various microstructural features. Morphology control of the porous structure also can be easily done by changing the solution properties and freezing conditions [21–23]. Many previous reports have shown improved performance when such devices are applied in energy devices [23–30]. Recently, the fabrication of cellular and lamellar $LiFePO_4$/C cathodes was reported [31]. However, the discussion of electrochemical properties of the lamellar structured $LiFePO_4$ is still insufficient.

Here, we suggest a well-aligned three-dimensional lamellar-structured $LiFePO_4$ electrode created via ice-templating and characterized the electrochemical performance by increasing active material loading. The ice-templated $LiFePO_4$ structure proposed here was composed of highly-aligned $LiFePO_4$ walls created by the packing of particles and macroscopic pore channels. The electrode design addresses the aforementioned issues and results in enhanced high rate capability than a conventional slurry-cast electrode. This new approach is potentially applicable to the development of porous electrode designs.

## 2. Experimental

Carbon-coated $LiFePO_4$ nanopowder (HED LFP-400, BASF) was used to create water-based slurry used here. The slurry was prepared with poly-acrylic acid (Partial sodium salt, 50 wt% solution in water, $M_w$ = 5000, Sigma-Aldrich, USA) as a dispersant system (LFP-400: PAA = 9:1 (wt.)) [32,33]. The concentration of $LiFePO_4$ powder in the final slurry was 20, 15, 10 vol%. The as-prepared slurry was dropped onto aluminum (thickness 0.25 mm, 99.999% trace metal basis, Sigma-Aldrich, USA) which was pretreated in 0.1 M phosphoric acid for 10 min as a hydrophilic treatment. Several drops on the aluminum plate (~1 $cm^2$) were covered by a hydrophobic-treated glass (Menzel-Glaser, 24 × 32 mm) and were frozen using liquid nitrogen. Subsequently, the glass was detached and the frozen sample was dried using a vacuum freeze dryer at −40 °C at 0.05 mbar for 0.5 h. When using the slurry with 15 and 20 vol% powders, the prepared slurry was stiff to fabricate the lamellar structure. For this reason, the slurry with 10 vol% powder was used to fabricate the ice-templated cathode. Finally, the freeze-dried sample was heated at a constant heating rate of 5 °C $min^{-1}$ to

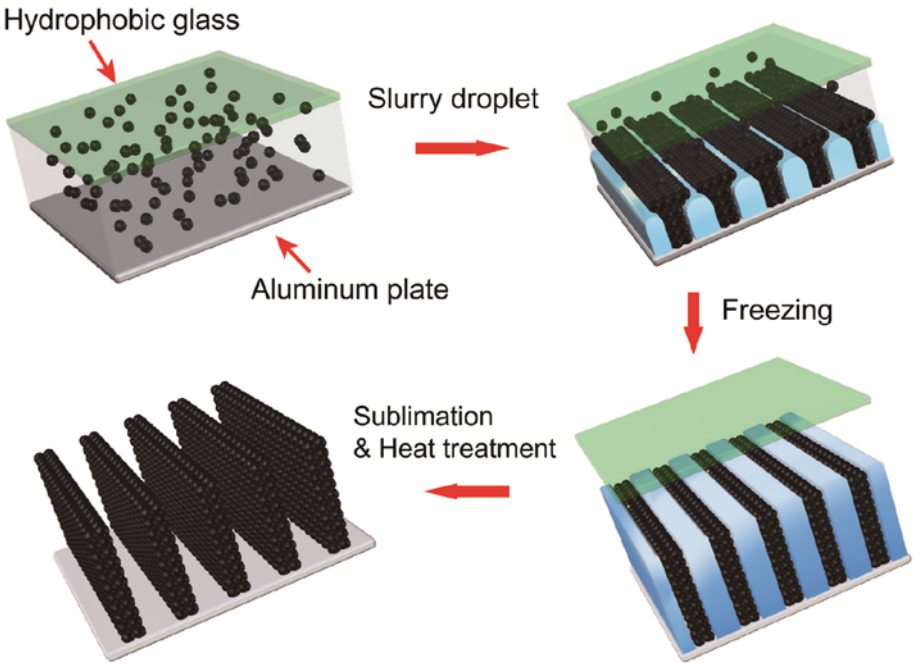


**Fig. 1.** Scheme of the fabrication process of ice-templated $LiFePO_4$ cathodes: Water-based slurry preparation, solidification, sublimation and heat treatment.

640 °C for 5 h in an argon atmosphere to carbonize the PAA polymer. The elemental analyzer (FLASH 2000 series) and transmission electron microscopy (FETEM Tecnai G2F30; FEI Company, Eindhoven, the Netherlands) was used to determine the amount of carbon in the LFP-400/Carbon mixture. The surface of the LFP-400 raw powder was coated with 2 wt% of carbon and the LFP-400/Carbon mixture then showed about 4 wt% of carbon. This occurred because the PAA polymer was changed to carbon (about 2 wt%) during the heat treatment to create a composite with $LiFePO_4$ walls (Table 1).

With the LFP-400/Carbon mixture, two cathode samples with different loading densities of 3 mg $cm^{-2}$ (FC_3) and 5 mg $cm^{-2}$ (FC_5) were prepared. The solid content contained in the $LiFePO_4$ slurry was fixed at 10 vol%, and it had a low tap density of approximately 25% of the theoretical $LiFePO_4$ density in both the FC_3 and FC_5 samples. Conventional slurry-cast cathodes were also prepared as control samples, referred to here as CS_3 and CS_5. In order to minimize differences in the heat treatment process between the ice-templated cathodes and the slurry casting cathodes, the LFP-400/Carbon mixture was used to fabricate CS series. The electrode slurry was prepared by mixing the LFP-400/Carbon mixture (90 wt%): Super P (5 wt%): poly vinylidene fluoride (5 wt%) and sonicated for 1 h to disperse all of the components homogenously. Detailed information about all of the samples is summarized in Table 2. The slurry was cast onto an aluminum foil by a doctor blade method followed by drying in a convection oven at 80 °C for 12 h. All of the cathodes were assembled into coin cells in an argon-filled glove box with Li anodes and 1 M $LiPF_6$ in ethylene carbonate (EC): dimethyl carbonate (DMC) [1:1 (vol%)] as an electrolyte with a separator (polypropylene film, Celgard Inc.).

The microstructure of the ice-templated cathode was characterized using a scanning electron microscope (FE-SEM Philips XL30 FEG). The electrochemical performance capabilities of the coin cells were tested via a high-precision battery performance testing system (WonATech, Korea, WBCS3000). The galvanostatic charge-discharge cycling performance of the cells was tested in the range of 2.2–4.2 V versus $Li^+/Li$ on a battery cycler at room temperature. The kinetics of the electrochemical reactions of the active materials was evaluated using two-

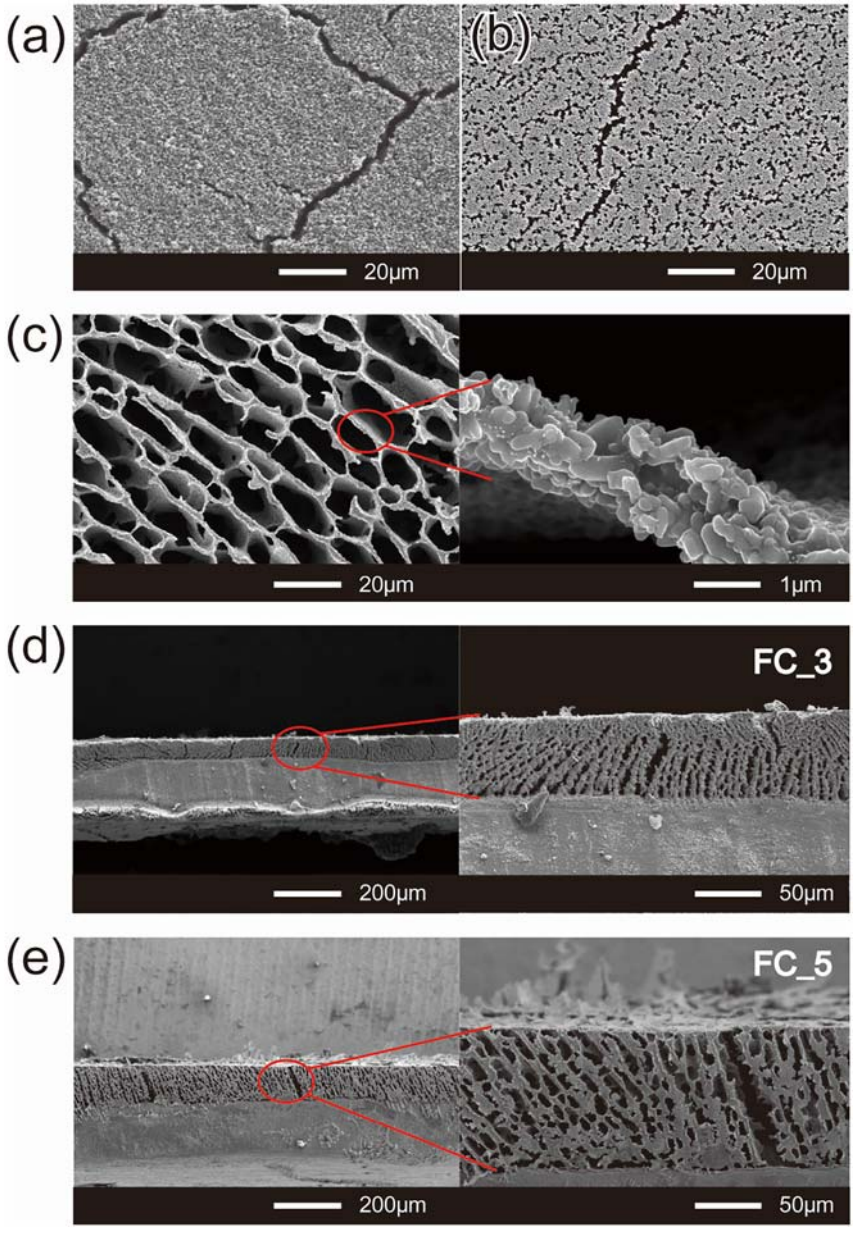


**Fig. 2.** SEM images of LiFePO4 cathodes: Ice-templated structure with (a) 20 vol% (b) 15 vol% and (c, d, e) 10 vol% water-based slurry, respectively. (c) Top view of lamellar structure (d) cross-section view of FC_3 and (e) FC_5.

probe AC impedance spectroscopy (Solartron 1260) in the frequency range of $10^6$ to 5 Hz with a scan rate of 0.1 mV/s.

## 3. Results & discussion

The scheme of the ice-templating procedure and the final lamellar structure of the cathodes are presented in Fig. 1. The $LiFePO_4$ nanoparticles and PAA are well dispersed in the slurry droplets. The PAA is a key material because the ice formulation and interaction between the particles and the solidification front can be modified through an additive system. Additive PAA clearly decreases the viscosity of the $LiFePO_4$ slurry and affects the ice formation process. When water is crystallized below its melting point, an ice pattern starts to form. The ice front velocity depends on the freezing direction, and the crystals grow to the final ice platelets due to the anisotropy of crystal growth kinetics [33]. During the growth of the ice crystal, the $LiFePO_4$ particles are segregated and entrapped between the platelet ice crystals, creating an aligned pattern. After sublimation, there remains a porous channel with highly-aligned $LiFePO_4$ walls. Finally, the ice-templated $LiFePO_4$ is heated in an argon atmosphere to improve the stability of the structure owing to interparticle necking.

When the slurry with 20 vol% $LiFePO_4$ nanopowder, the viscosity dramatically increased and became stiff. The increase in viscosity caused less expansion of the ice crystal during the freezing, resulted in an increase in the density of active material as shown in Fig. 2(a). The slurry with 15 vol% $LiFePO_4$, the cellular-like porous structure is shown because the overall expansion of ice crystal increased by decreasing viscosity (Fig. 2(b)). The optimized slurry concentration is around 10 vol% which results in the lamellar structure (Fig. 2(c–e)). A top view of the fabricated $LiFePO_4$ cathode shows that the $LiFePO_4$ wall width is approximately 1.2 μm and that the spacing between the walls is about 8–9 μm, matching the expected results when considering the 10 vol% concentration of the initial $LiFePO_4$ slurry (Fig. 2(c)). Under high magnification, it appears that each highly-aligned wall has randomly stacked $LiFePO_4$ nanoparticles with necking after the heat treatment. Each SEM image in Fig. 2(d) and (e) also presents a cross-section view of FC_3 and FC_5 on the aluminum current collector. The average heights of the walls of the FC_3 and FC_5 samples are approximately 60 μm and 110 μm, respectively. Under high magnification, the adhesion between the active material and substrate appears to be good enough to support a continuous electron path, leading to stable electrochemical performance, as shown in Fig. 5(c). The $LiFePO_4$ film thickness and structure of the final product clearly are sufficiently homogeneous for the fabrication of coin cells.

The PAA can be carbonized during the heat treatment, covering each of the $LiFePO_4$ walls. The elemental analysis (Table 1) shows the amount of carbon in the LFP-400/Carbon composites after carbonization as shown in previous reports [34]. The TEM images of the raw powder LFP-400 and LFP/Carbon are expressed in Fig. 3. The carbonized PAA forms a larger amount of carbon around the LFP-400 particles. It is expected that the partially sintered $LiFePO_4$ particles and carbonized PAA during the heat treatment enhance electric conductivity.

All electrochemical performance capabilities of the $LiFePO_4$ cathodes are tested by fabricating coin cells. As shown in Fig. 4(a) and (c), the discharge capacities at different rates are compared between FC_3 and CS_3 from 2.2 to 4.2 V (vs. $Li/Li^+$). The current densities used for the discharge are 85.5 mA $g^{-1}$ (0.5 C) and 3.42 A $g^{-1}$ (20C), respectively. The specific discharge capacity of FC_3 is close to 130 mAh $g^{-1}$ at 0.5 C. The specific discharge capacity of FC_3 is about 93 mAh $g^{-1}$ at a 20C-rate, exhibiting less of a decrease in the specific capacity with a low overpotential compared to the value of CS_3 (80 mAh $g^{-1}$). Moreover, it is apparent that the advantage of the ice-templated structure is remarkable when increasing the loading density of the active materials (Fig. 4(b) and (d)). The FC_5 sample shows a low discharge overpotential in spite of the high rate and high

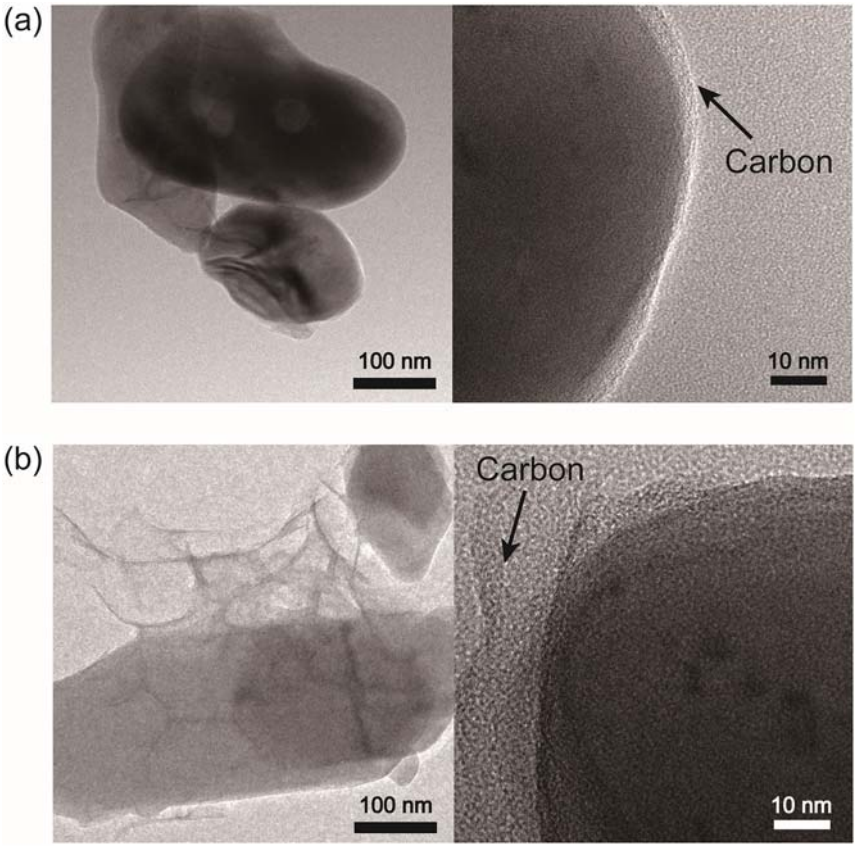


**Fig. 3.** TEM images of (a) raw powder $LiFePO_4$ and (b) LFP/C composites after carbonization of PAA.

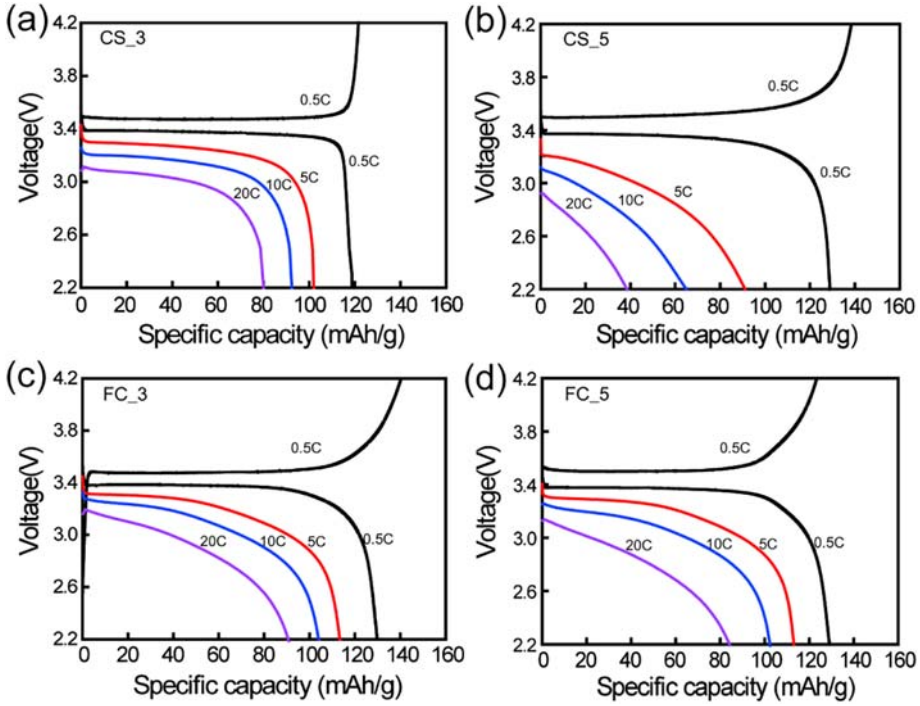


**Fig. 4.** Galvanostatic charge and discharge curves at various current densities at 0.5 to 20 C-rate for (a) CS_3 (b) CS_5 (c) FC_3 and (d) FC_5.

loading density. On the other hand, the CS_5 sample shows a high overpotential as well as a low discharge capacity under high rate conditions. The specific capacities of CS_5 and FC_5 are close to 40 mAh $g^{-1}$ and 85 mAh $g^{-1}$ at 20C-rate, respectively. This result indicates that the ice-templated cathode with a small degree of a carbon additive system enhanced the rate performance significantly. The three-dimensional ordered porous structure coating with the conductive material facilitates rapid electron transfer into the $LiFePO_4$ frame wall, and the electrolyte makes even contact with the electrode. In addition, the electron is not interrupted by any non-conductive binder such as polyvinylidene fluoride because the process only contains $LiFePO_4$ powder and carbon. The superior electric conductivity in the $LiFePO_4$ lamellar structure decreases the overpotential, especially when using an electrode with a high loading density, indicating that the increase in the thickness of the freeze-casted $LiFePO_4$ wall from 60 to 110 μm is not crucial for electric conductivity, while the thickness of the

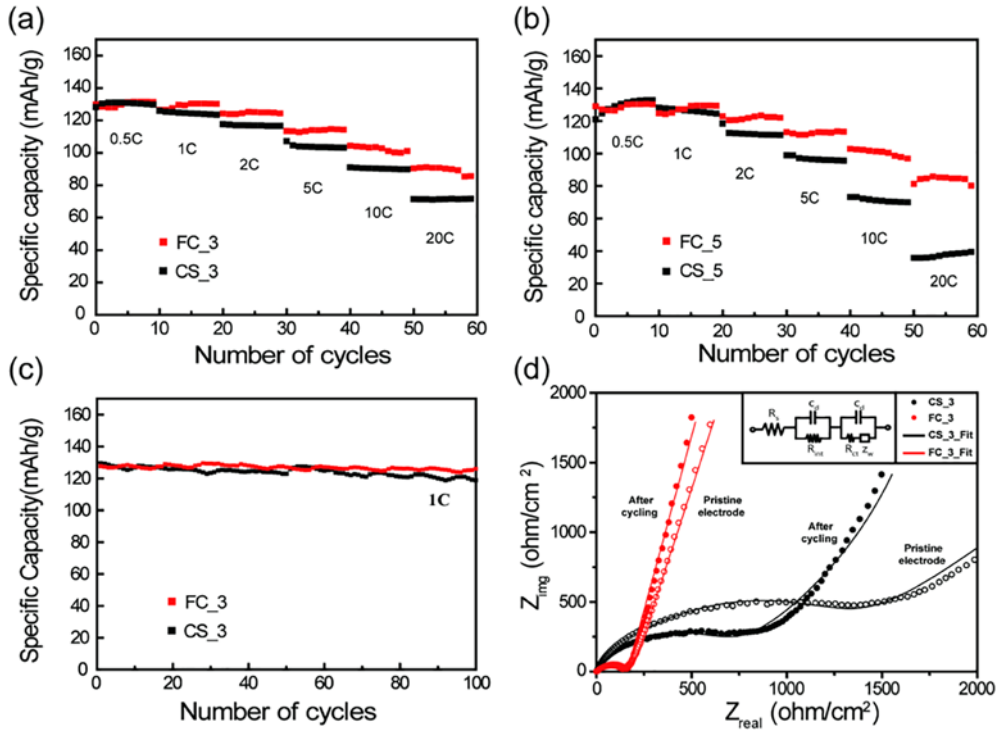


**Fig. 5.** Rate capability curves of (a) FC_3 and CS_3 (b) FC_5 and CS_5. (c) Cycling performance of FC_3 and CS_3 at a constant 1C-rate for 100 cycles. (d) Nyquist plots of pristine CS_3 (1549.8 Ω $cm^{-2}$) and FC_3 (157.6 Ω $cm^{-2}$) electrode. After 100 cycle: CS_3 (970.1 Ω $cm^{-2}$) and FC_3 (138.1 Ω $cm^{-2}$).

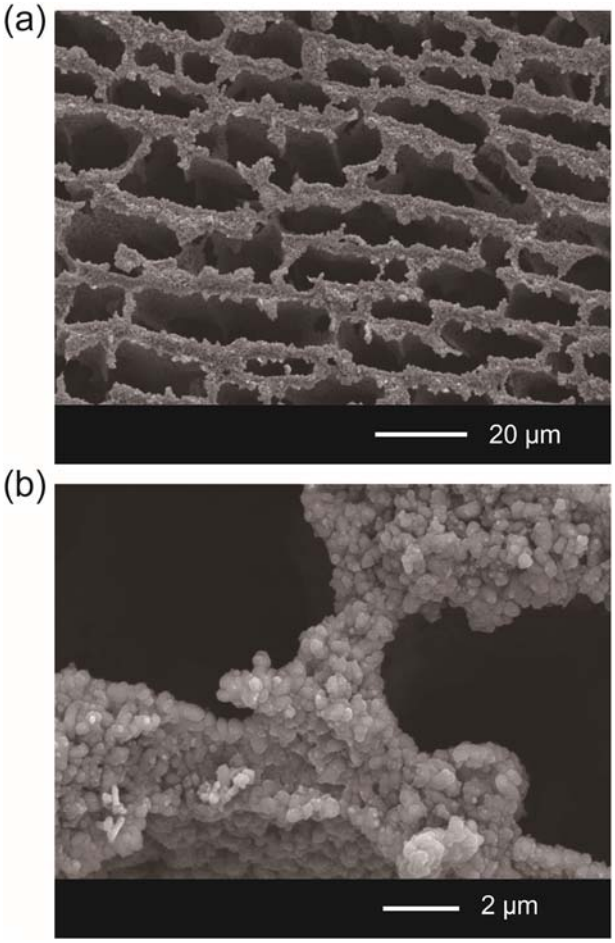


**Fig. 6.** Ex-situ SEM observation of the FC_3 cathode after 100 cycles: (a) top view under low magnification, and (b) top view under high magnification.

conventional slurry-cast cathode method considerably affects the electric conductivity. The high discharge capacity at a high rate can be attributed to the increased electric conductivity and better electrolyte contact with the electrode.

The discharge capacity of FC_5 shows higher than the charge capacity under 0.5 C. The previous work also presented that the first charge capacity is lower than discharge capacity in case of $LiFePO_4$ [35]. They explained why some lithium ions cannot be fully extracted from the ordered-olivine structure which in turn causes some charge capacity loss. The first one is limited lithium ion phase-boundary diffusion due to the ionic disorder such as stacking faults, and second one is low electron conductivity. These problems could make the limitation of the $Li^+$ extraction.

The rate capability studies of the FC and CS series are presented in Fig. 5(a) and (b). As the rate increases, the difference in the specific capacity between FC_3 and CS_3 also increases. Moreover, FC_5 shows a much better rate capability than CS_5, retaining a high value of 85 mAh $g^{-1}$ at 20C. The cycleability of the FC_3 sample is compared with that of the CS_3 sample, as shown in Fig. 5(c), illustrating the stability of the cell composed of the ice-templated cathodes. Cycle stability is clearly good considering the decreasing slope, and after 100 cycles, the discharge capacity is nearly 96.7% of its initial capacity. The freeze-casted $LiFePO_4$ cathode is rigid enough to maintain a porous lamellar structure after 100 cycles. Electrochemical impedance spectra (EIS) curves of the CS_3 and FC_3 were obtained before and after 100 cycles to investigate the effects of lamellar structured cathode. The Fig. 5(d) shows the EIS profiles consisting of a partially overlapped semicircle in the high frequency region that describes the charge transfer resistance ($R_{ct}$), followed by a sloping line in the low frequency region, which could be considered as Warburg impedance ($Z_w$), which is associated with Li-ion diffusion in the bulk of the electrode [36–38]. The resistance was measured by fitting the impedance spectrum with the equivalent model combining the diameters of the semicircles, and these values are 970.1 Ω $cm^{-2}$ for CS_3 and 138.1 Ω $cm^{-2}$ for FC_3 after 100 cycles. The impedance of the FC_3 is smaller than that of CS_3 indicating lower charge resistance of FC_3. Furthermore, the impedance slopes of FC_3 in the low frequency range are also much higher than that of the CS_3 cathode, reflecting better kinetics for ionic conductivity of the FC_3 cathode.

The morphology is observed after 100 charge-discharge cycles to confirm the structural stability of the ice-templated $LiFePO_4$ cathodes (Fig. 6). This result shows that the lamellar-structured cathode remains nearly identical after the electrochemical reaction. It is considered that the structure can be maintained without a binder system owing to the strong bonding between the aluminum current collector and the lamellar structure arising from the heat treatment process. Taking into account the results from the electrochemical performance and morphology assessments of the ice-templated cathode structure, the electron mean free path and electrolyte contact area according to the cathode structure are illustrated in Fig. 7. The tape-casted cathode shows randomly distributed particles mixed with binders which deteriorate the rate performance due to the low lithium ion permeability and the long mean free path of the electrons. On the other hand, the ice-templated cathode has a highly-aligned lamellar structure, which is advantageous for lithium ion permeability and for the electron path to the current collector.

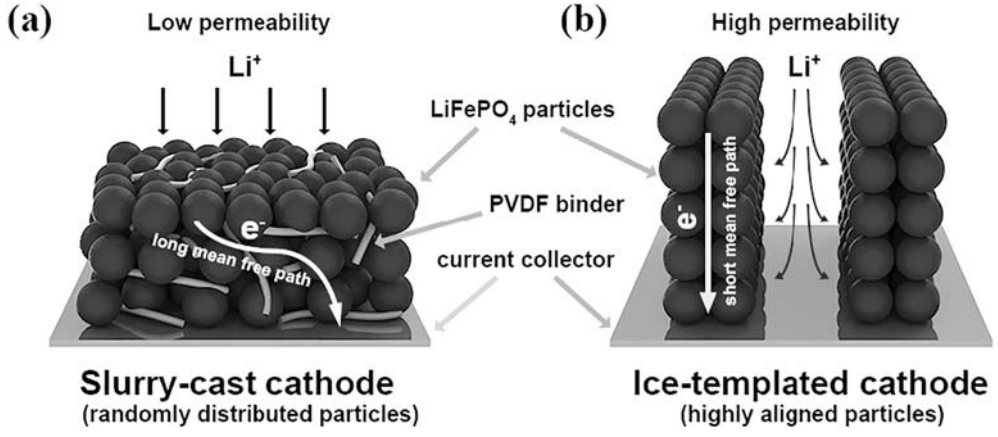


**Fig. 7.** Scheme of the cathode structures considering the electron pathways and lithium ion permeability: (a) conventional slurry-cast cathode, and (b) ice-templated cathode.

## 4. Conclusions

An aqueous slurry-based ice-templating method was introduced to create a highly-aligned porous $LiFePO_4$ structure for a Li-ion battery cathode. The ice-templated lamellar structure was a well-aligned three-dimensional porous structure, and the fabricated electrode showed better electrochemical performance at a high C rate, with a specific capacity of 93 mAh $g^{-1}$ at 20 C-rate. In addition, the structure remarkably improved the electrochemical performance with a higher loading density and a high C-rate. These results suggest that the highly-aligned porous $LiFePO_4$ structure has good electric conductivity and lithium ion conductive paths, which likely explain why it exhibited better high-rate performance compared to conventional slurry-cast cathodes.

## Acknowledgments

This work was supported by Pioneer Research Center Program (2011-0001684), National Research Foundation of Korea (NRF) funded by the Korean government (MSIT) (No. 2017R1A2B2010148). It was also supported by the Climate Change Research Hub of KAIST (Grant No. N11170059).

## References

[1] Y.-H. Liu, M. Okano, T. Mukai, K. Inoue, M. Yanagida, T. Sakai, J. Power Sources 304 (2016) 9–14.
[2] J. Zhang, L. Su, Z. Li, Y. Sun, N. Wu, Batteries 2 (2016) 12.
[3] C. (John) J. Zhang, S.H. Park, S.E. O'Brien, A. Seral-Ascaso, M. Liang, D. Hanlon, D. Krishnan, A. Crossley, N. McEvoy, J.N. Coleman, V. Nicolosi, Nano Energy 39 (2017) 151–161.
[4] Y. Chen, K. Fu, S. Zhu, W. Luo, Y. Wang, Y. Li, E. Hitz, Y. Yao, J. Dai, J. Wan, V.A. Danner, T. Li, L. Hu, Nano Lett. 16 (2016) 3616–3623.
[5] J. Hu, W. Li, Y. Duan, S. Cui, X. Song, Y. Liu, J. Zheng, Y. Lin, F. Pan, Adv. Energy Mater. 7 (2017) 1–10.
[6] B. Wang, W. Al Abdulla, D. Wang, X.S. Zhao, Energy, Environ. Sci. 8 (2015) 869–875.
[7] B. Wang, T. Liu, A. Liu, G. Liu, L. Wang, T. Gao, D. Wang, X.S. Zhao, Adv. Energy Mater. 6 (2016) 1–10.
[8] Z. Wu, S. Ji, T. Liu, Y. Duan, S. Xiao, Y. Lin, K. Xu, F. Pan, Nano Lett. 16 (2016) 6357–6363.
[9] S. Wang, L. Xia, L. Yu, L. Zhang, H. Wang, X.W. Lou, Adv. Energy Mater. 6 (2016) 1–7.
[10] Y. Zheng, T. Zhou, C. Zhang, J. Mao, H. Liu, Z. Guo, Angew. Chem. Int. Ed. 55 (2016) 3408–3413.
[11] C. Liu, C. Li, K. Ahmed, Z. Mutlu, C.S. Ozkan, M. Ozkan, Sci. Rep. 6 (2016) 29183.
[12] K. Zhao, L. Zhang, R. Xia, Y. Dong, W. Xu, C. Niu, L. He, M. Yan, L. Qu, L. Mai, Small 12 (2016) 588–594.
[13] K. Ui, S. Kikuchi, F. Mikami, Y. Kadoma, N. Kumagai, J. Power Sources 173 (2007) 518–521.
[14] J. Li, C. Daniel, D. Wood, J. Power Sources 196 (2011) 2452–2460.
[15] Z.P. Cai, Y. Liang, W.S. Li, L.D. Xing, Y.H. Liao, J. Power Sources 189 (2009) 547–551.
[16] C.J. Bae, C.K. Erdonmez, J.W. Halloran, Y.M. Chiang, Adv. Mater. 25 (2013) 1254–1258.
[17] A. Vu, Y. Qian, A. Stein, Adv. Energy Mater. 2 (2012) 1056–1085.
[18] S. Moon, Y.H. Jung, W.K. Jung, D.S. Jung, J.W. Choi, D.K. Kim, Adv. Mater. 25 (2013) 6547–6553.
[19] C. Wu, J. Maier, Y. Yu, Adv. Mater. 28 (2016) 174–180.
[20] D. Li, W. Zhang, R. Sun, H.-T.-H. Yong, G. Chen, X. Fan, L. Gou, Y. Mao, K. Zhao, M. Tian, Nano 8 (2016) 12202–12214.
[21] D.S. Kim, D.K. Kim, Int. J. Appl. Ceram. Technol. 12 (2015) 921–931.
[22] S. Deville, J. Mater. Res. 28 (2013) 2202–2219.
[23] K.H. Lee, Y.-W. Lee, S.W. Lee, J.S. Ha, S.-S. Lee, J.G. Son, Sci. Rep. 5 (2015) 13696.
[24] H. Zhang, I. Hussain, M. Brust, M.F. Butler, S.P. Rannard, A.I. Cooper, Nat. Mater. 4 (2005) 787–793.
[25] Y. Chen, J. Bunch, T. Li, Z. Mao, F. Chen, J. Power Sources 213 (2012) 93–99.
[26] D.S. Kim, C. Baek, H.J. Ma, D.K. Kim, Ceram. Int. 42 (2015) 7141–7147.
[27] Y. Shao, M.F. El-Kady, C.W. Lin, G. Zhu, K.L. Marsh, J.Y. Hwang, Q. Zhang, Y. Li, H. Wang, R.B. Kaner, Adv. Mater. (2016) 6719–6726.
[28] S.W. Sofie, J. Am. Ceram. Soc. 90 (2007) 2024–2031.
[29] W. Zhang, X. He, W. Pu, J. Li, C. Wan, Ionics (Kiel) 17 (2011) 473–477.
[30] K. Lu, C.S. Kessler, R.M. Davis, J. Am. Ceram. Soc. 89 (2006) 2459–2465.
[31] S. Zavareh, A. Hilger, K. Hirselandt, O. Goerke, I. Manke, J. Banhart, A. Gurlo, J. Ceram. Soc. Japan 124 (2016) 1067–1071.
[32] J. Lee, H. Kim, S.B. Wee, U. Paik 27 (2009) 239–245.
[33] S. Deville, Adv. Eng. Mater. 10 (2008) 155–169.
[34] C. Kim, Y.J. Cho, W.Y. Yun, B.T.N. Ngoc, K.S. Yang, D.R. Chang, J.W. Lee, M. Kojima, Y.A. Kim, M. Endo, Solid State Commun. 142 (2007) 20–23.
[35] B. Lung-Hao Hu, F.-Y. Wu, C.-T. Lin, A.N. Khlobystov, L.-J. Li, Nat. Commun. 4 (2013) 1687.
[36] S.H. Jo, P. Muralidharan, D.K. Kim, J. Alloys Compd. 491 (2010) 416–419.
[37] S.J. Lee, D.S. Kim, S.H. Jo, P. Muralidharan, D.K. Kim, Ceram. Int. 38 (2012) S493–S496.
[38] S.J. Lee, D.S. Kim, P. Muralidharan, S.H. Jo, D.K. Kim, J. Power Sources 196 (2011) 3095–3098.